

Indole–1,2,4-triazole hybrids as selective ERK inhibitors: Synthesis, anticancer evaluation, and molecular modeling**Mohamed G. Abouelenein^{a*}, Yasmin K. Elsersty^a, Hayam A. Abd El Salam^b, Hanem M. Awad^c, Zeinab A. El-Shahid^d, Mohammed T. Abdel-Aal^a and Heba M. Abo-Salem^e**^aChemistry Department, Faculty of Science, Menoufia University, Shebin El-Koam, Menoufia, Egypt^bGreen Chemistry Department, Organic Chemicals Industries Institute National Research Centre, Dokki, Giza, 12622, Egypt^cChemistry of Tanning Materials and Leather Technology Department, Organic Chemicals Industries Institute, National Research Centre, Dokki 12622, Cairo, Egypt^dChemistry of Natural and Microbial Products Department, Pharmaceutical and Drug Industries Research Institute, National Research Centre, Dokki, Giza 12622, Egypt^eChemistry of Natural Compounds Department, Pharmaceutical and Drug Industries Research Institute, National Research Centre, Dokki, 12622 Giza, Egypt**CHRONICLE***Article history:*

Received March 10, 2025

Received in revised form

June 2, 2025

Accepted July 7, 2025

Available online

July 7, 2025

*Keywords:**Indole-3-propionic acid**Anticancer agents**Cytotoxicity**ERK kinase**Molecular docking**ADMET***ABSTRACT**

A new series of structurally diverse indole–1,2,4-triazole derivatives was designed and synthesized through a thiolated triazole intermediate derived from indole-3-propionic acid. The final compounds, including *S*-acetamide, bis-indolyl, triazolothiadiazole, and triazolothiadiazine analogues (**3–8**), were confirmed by NMR, IR, MS, and elemental analysis. Their cytotoxicity was tested against breast (MCF-7), colon (HCT-116), and liver (HepG2) cancer cell lines, alongside normal BJ-1 fibroblasts, using the LDH assay. Several compounds, especially **3**, **6b**, **7a**, **7c**, and **8a,b** showed potent and selective antiproliferative effects on MCF-7 and HCT-116 cells with IC₅₀ values between 2.3 and 3.0 μM, outperforming doxorubicin nearly twofold under the same conditions. Mechanistic studies revealed a significant decrease in phosphorylated ERK (pERK) protein levels in MCF-7 cells, with compound **3b** showing the strongest inhibition (3.499 ± 0.21 pg/mL), consistent with its IC₅₀ (2.3 μg/mL). Molecular docking supported the strong binding affinity of **3b** within the ERK active site (−9.0 kcal/mol), involving hydrogen bonding and hydrophobic interactions. *In silico* ADMET predictions confirmed favorable drug-likeness, oral bioavailability, and pharmacokinetic safety for this compound. Overall, compound **3b** emerges as a promising lead for ERK-targeted anticancer drug development, supported by combined synthetic, biological, and computational evidence.

© 2025 by the authors; licensee Growing Science, Canada.

1. Introduction

Cancer is a complex and heterogeneous disease caused by disruption in cellular mechanisms that regulate proliferation and apoptosis. This disruption leads to uncontrolled cell growth, resulting in tumor formation in both solid tissues and blood systems.^{1,2} Despite major advances in early detection and treatment, cancer remains a leading global health problem. In 2020, it caused nearly 10 million deaths worldwide, ranking second after cardiovascular diseases.^{3,4} Current treatments include surgery, radiotherapy, immunotherapy, and chemotherapy.⁵ Among these, chemotherapy is still a primary clinical approach. However, its use is limited by systemic toxicity, low selectivity, and the development of multidrug resistance. These challenges have motivated the search for new chemotherapeutic agents that offer higher efficacy with improved safety. In recent years, cancer therapy has shifted towards molecularly targeted strategies that focus on signaling pathways dysregulated in cancer cells.^{6,7} One key target is the extracellular signal-regulated kinase (ERK), a vital part of the mitogen-activated protein kinase (MAPK) pathway. ERK regulates essential cellular processes including proliferation, differentiation, survival, and migration.⁸ Abnormal activation of the MAPK/ERK pathway is linked to many cancers,

* Corresponding author

E-mail address moh.gamal89@yahoo.com (M. G. Abouelenein)

neurodegenerative disorders, and metabolic diseases.⁸ Because ERK is involved in over 30% of human cancers, it is considered a promising target for next-generation anticancer drugs.⁹

Heterocyclic compounds, especially nitrogen-containing scaffolds, are central in drug discovery. Nearly 75% of FDA-approved drugs contain such structures.^{10,11} Among these, the indole ring is notable for its diverse pharmacological effects, including antimicrobial, anti-inflammatory, and anticancer properties.^{12,13} Several indole-based compounds have shown strong activity against tumors such as breast cancer, leukemia, lymphoma, and small-cell lung carcinoma.¹⁴⁻¹⁸ This establishes indole as a key motif in anticancer drug design. Similarly, 1,2,4-triazoles have gained attention due to their chemical stability, hydrogen bonding ability, and capacity to affect biological targets.^{19,20} The 1,2,4-triazole ring is found in several approved anticancer drugs like letrozole, anastrozole, and vorozole, which are used against hormone-dependent breast cancer (**Fig. 1**). This scaffold enhances binding affinity, selectivity, and metabolic stability. Moreover, the bioactivity of these heterocycles is strongly influenced by the presence of nitrogen-containing five-membered rings, such as the triazole moiety, which act as privileged pharmacophores in modulating biological targets through electronic effects and strong hydrogen bonding.²¹⁻²³

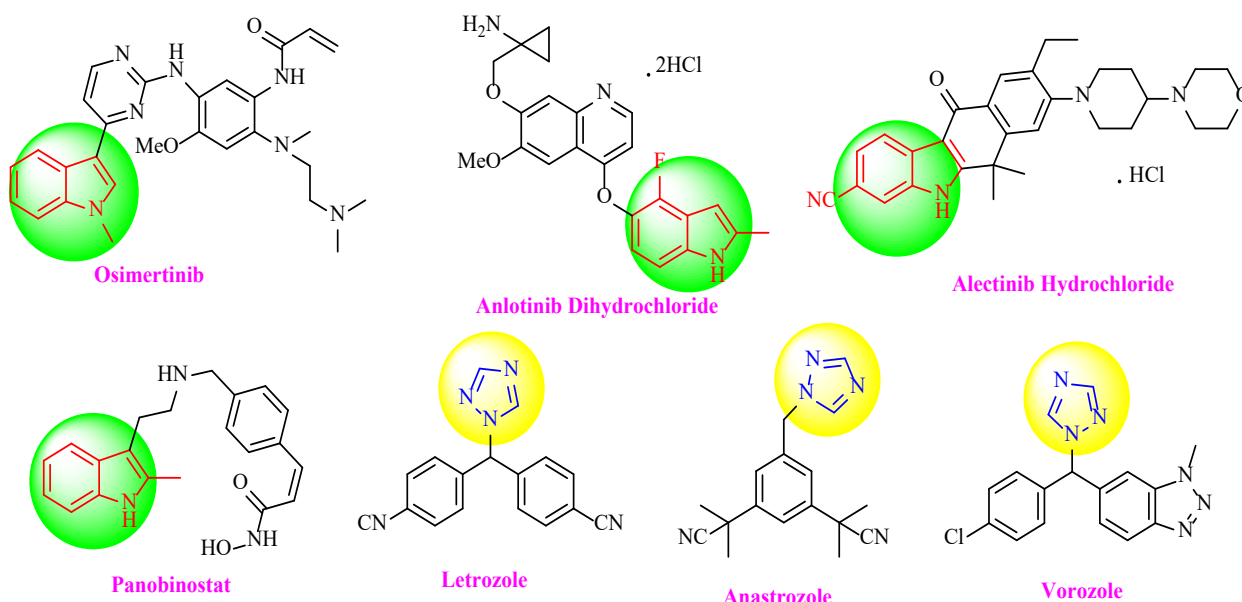


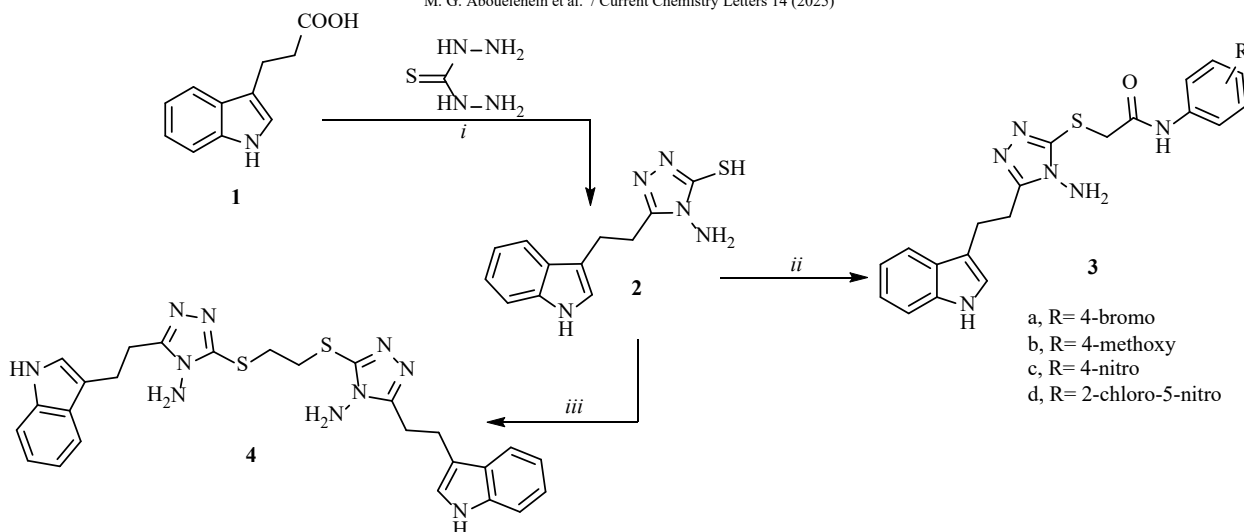
Fig. 1. Chemical structure of some indole and 1,2,4-triazole based anti-cancer drugs

Recent research shows that hybrid molecules combining indole and 1,2,4-triazole units can achieve stronger anticancer effects through synergistic action.^{24,25} This hybridization merges two bioactive groups into one molecule, improving pharmacokinetics, target specificity, and overall therapeutic effect. Building on our ongoing work to discover new heterocyclic compounds with anticancer potential,²⁶⁻³¹ this study reports the synthesis and biological evaluation of novel indole–1,2,4-triazole hybrids. The compounds were tested for cytotoxicity against MCF-7 (breast), HCT-116 (colon), and HepG2 (liver) cancer cells, as well as BJ-1 normal fibroblasts, using the LDH release assay. The most active derivatives were further assessed for their ability to inhibit phosphorylated ERK (pERK) levels. Molecular docking was also performed to investigate binding with ERK, and *in silico* ADMET profiling evaluated drug-likeness and pharmacokinetic safety.

2. Results and Discussion

2.1 Chemistry

Indole–triazole hybrids have emerged as privileged scaffolds in modern heterocyclic chemistry, combining the pharmacophoric richness of indole with the versatile reactivity of 1,2,4-triazoles. Their unique structural adaptability enables the construction of multifunctional molecules with potential applications spanning synthetic, medicinal, and materials chemistry. The new indole–triazole hybrids (**3–8**) were synthesized following the strategies shown in **Scheme 1** and **Scheme 2**. The key intermediate 5-(2-(1*H*-indol-3-yl)ethyl)-4-amino-4*H*-1,2,4-triazole-3-thiol (**2**) was obtained from indole-3-propionic acid (**1**) and thiocarbohydrazide under fusion conditions. This 4-amino-4*H*-1,2,4-triazole-3-thiol congener (**2**) served as a versatile branching point for subsequent functionalization. In **Scheme 1**, the thiol derivative **2** was *S*-alkylated *via* coupling reaction with various α -chloroacetamides, namely 4-*N*-(4-bromophenyl)-2-chloroacetamide, 2-chloro-*N*-(4-methoxyphenyl)acetamide, 2-chloro-*N*-(4-nitrophenyl)acetamide, and 2-chloro-*N*-(2-chloro-5-nitrophenyl)acetamide, to yield the corresponding *S*-acetamide derivatives **3a–3d**.



Scheme 1. Synthesis of 1,2,4-triazole derivatives **2-4**, reagents and conditions: (i) Oil bath, fusion at 130–140 °C for 4h; (ii) Chloro acetamide derivatives, acetone, K_2CO_3 , reflux, (iii) 1,2-Dibromoethane, dry acetone, K_2CO_3 .

The success of this transformation was confirmed by NMR spectroscopy. In the 1H NMR spectra of **3a–3d**, the characteristic $-SH$ proton of compound **2** (δ 13.43 ppm) is absent, and new signals appeared for the triazole NH, the amine NH_2 , and the amide functionalities. For example, compound **3b** (derived from 4-methoxyphenyl chloroacetamide) shows singlet signals at δ 10.78 ppm and 10.20 ppm (each 1H), assignable to the triazole NH and the amide NH, respectively, and a singlet signal at δ 5.93 ppm integrating to 2H (the triazole NH_2). A distinct singlet at δ 3.69 ppm (3H) corresponds to the methoxy group, and another at δ 4.01 ppm (2H) corresponds to the CH_2 moiety of the acetamide side chain. The ethylene linker between indole and triazole appears as multiplets at δ 3.03–3.01 ppm (4H total), and the aromatic protons of the indole and phenyl rings resonate between δ 6.9–7.5 ppm. In the ^{13}C NMR spectrum of **3b**, the carbonyl carbon appears at δ ~170.8 ppm, the OCH_3 carbon at δ 56.8 ppm, and three CH_2 carbons at δ 44.0, 26.5, and 22.4 ppm, in agreement with the expected structure. Analogous NMR patterns for **3a**, **3c**, and **3d** confirmed the *S*-acetamide structures of these analogues.

Also in **Scheme 1**, reaction of compound **2** with 1,2-dibromoethane (in dry acetone, K_2CO_3) gave the *bis*(indolyl)triazole **4**. In the 1H NMR spectrum of **4** ($DMSO-d_6$), the thiol signal is absent, and the spectrum exhibits a singlet NH signal at δ 10.78 ppm (1H) and two NH_2 signals as broad singlets at δ 5.90 ppm (2H) and δ 5.32 ppm (2H). These resonances correspond to the triazole NH and the two primary NH_2 groups of the di-triazole structure. The six methylene protons from the two ethylene linkers appear as overlapping multiplets between δ 2.8–3.0 ppm (total 12H), and the aromatic region (δ 6.9–7.8 ppm) accounts for ten protons from the two indole rings. The ^{13}C NMR spectrum of **4** shows six aliphatic carbon signals at δ 31.6, 26.5, 25.6, 25.2, 22.8, and 22.3 ppm, consistent with three pairs of CH_2 groups. Together, these data confirm the symmetrical *bis*-indolyl structure of **4**.

In **Scheme 2**, cyclization of **2** with carbon disulfide (KOH/MeOH, reflux) afforded the fused triazolo[3,4-*b*][1,3,4]thiadiazole-6-thiol **5**. The 1H NMR spectrum of **5** ($DMSO-d_6$) shows disappearance of the NH_2 resonances present in **2** and the emergence of a new singlet signal at δ 12.50 ppm (1H) due to the thiol proton in **5**. A triazole NH resonance appears at δ 10.84 ppm (1H), and the ethylene linker protons are observed as multiplets around δ 3.0 ppm (total 4H). The aromatic indole protons are seen between δ 6.9–7.8 ppm. These shifts are fully consistent with the formation of the thiadiazole ring. The ^{13}C NMR exhibits a characteristic resonance for the $C=S$ of indole, triazole and ethylene carbon atoms (experimental section), further supporting the assigned structure of **5**.

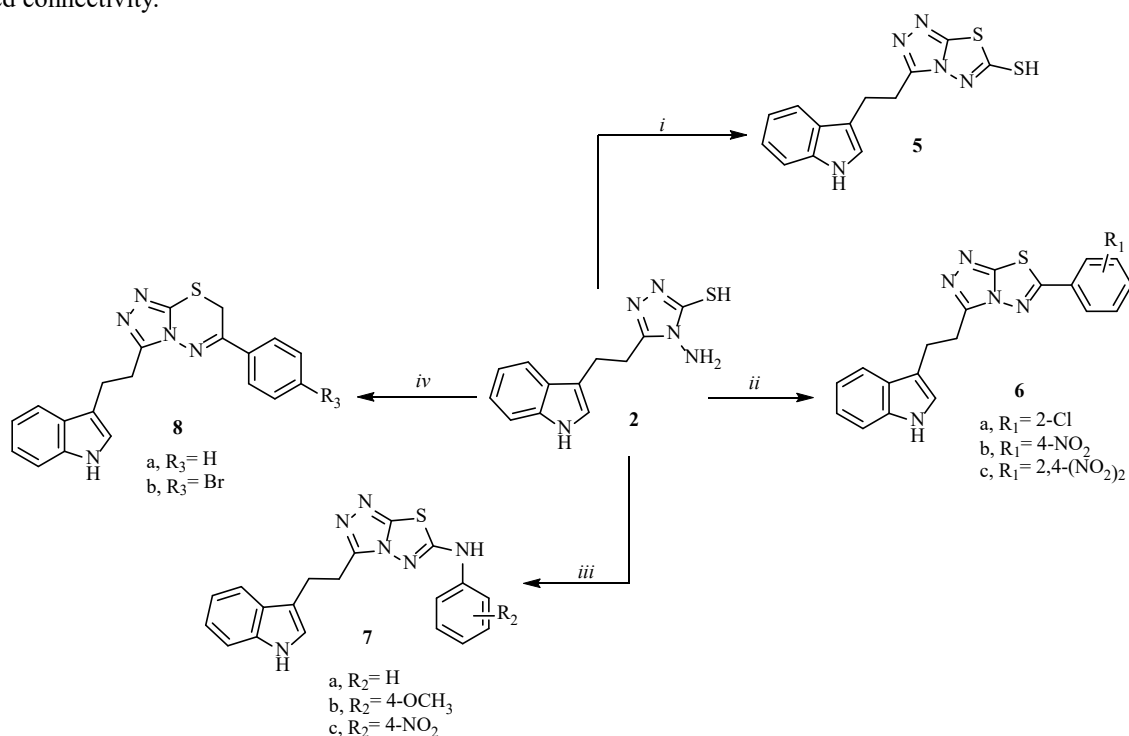
Compound **2** was also cyclized with substituted benzoic acids (i.e. 2-chloro or 4-nitro benzoic acids) or 2,4-dinitro benzoyl chloride under reflux in $POCl_3$ to give the triazolo[3,4-*b*][1,3,4]thiadiazoles **6a–6c**. The 1H NMR spectra of **6a–6c** each display a single NH singlet (δ 10.97, 10.78, 10.96 ppm) and lack any NH_2 or SH signals, indicating successful ring closure. For example, compound **6b** (4-nitrophenyl) shows a singlet at δ 10.78 ppm (1H, NH) and aromatic multiplets at δ 8.97–8.80 ppm (4H, Ar-H) and δ 7.24–6.92 ppm for 5H. The CH_2-CH_2 linker resonates at δ 3.01 ppm (4H). In the ^{13}C NMR of **6b**, peaks appear at δ 164.5, 153.2, 26.50, and 22.36 ppm, assignable to the $C=N$, CH_2 carbons, respectively, and the aromatic carbons are consistent with the nitrophenyl and indolyl moieties. These data confirm the thiadiazole-fused triazole structure of **6b** (and similarly for **6a** and **6c**).

Similarly, reaction of **2** with aryl isothiocyanates, namely phenyl isothiocyanate, 4-methoxy and 4-nitro phenyl isothiocyanates under reflux in DMF afforded the triazolo[3,4-*b*][1,3,4]thiadiazol-6-amine derivatives **7a–7c**. In these compounds, the 6-position of the fused ring bears an arylamino group. Their 1H NMR spectra all feature two NH signals (total integration 2H) around δ 10.77, 10.76 ppm, corresponding to the indole NH and the aniline NH. For instance, **7b** (4-methoxyphenylamine) shows a broad singlet at δ 10.76 ppm (2H, 2NH), a singlet at δ 3.74 ppm (3H, OCH_3 of the anisyl

group), and aromatic signals at δ 7.68–7.03 ppm (9H). The ethylene linker protons appear at δ 3.01–2.88 ppm (4H). The ^{13}C NMR of **7b** displays the methoxy carbon at δ 51.7 ppm and characteristic aromatic and aliphatic signals, consistent with the assigned structure. Compounds **7a** (phenyl) and **7c** (nitrophenyl) show analogous ^1H NMR patterns (e.g. singlets at δ ~10.77 ppm and aromatic multiplets), supporting their structures.

Finally, treatment of **2** with *p*-bromophenacyl bromide in ethanol utilizing K_2CO_3 as a catalyst produced the 7*H*-[1,2,4]triazolo[3,4-*b*][1,3,4]thiadiazine derivatives **8a** and **8b** (Scheme 2). In the ^1H NMR of **8a** (unsubstituted phenyl), the NH_2 and SH signals are absent, and an NH singlet appears at δ 10.77 ppm (1H). A singlet at δ 7.91 ppm (1H) corresponds to the indole H-2, while a new singlet at δ 4.00 ppm (2H) is assignable to the CH_2 group within the thiadiazine ring. The remaining aromatic and $\text{CH}_2\text{--CH}_2$ protons give multiplets at δ 7.29–6.93 and 3.04–2.71 ppm (4H). In **8b** (4-bromophenyl), the pattern is similar (NH at δ 10.76 ppm, CH_2 at δ 4.00 ppm, $\text{CH}_2\text{--CH}_2$ at δ 3.05, and aromatic protons at δ 7.57–7.03 ppm). These chemical shifts and coupling patterns are consistent with formation of the triazolothiadiazine scaffold.

In summary, the synthetic sequences delivered the target compounds **3a–3d** and **4–8**, and each was thoroughly characterized by spectroscopic analysis. The complete ^1H and ^{13}C NMR data discussed above unambiguously confirm the structures of all new hybrids, with each key functional group resonating at the expected chemical shift according to the proposed connectivity.



Scheme 2. Synthesis of 1,2,4-triazole derivatives **5–8**, reagents and conditions: (i) Carbon disulfide, KOH/MeOH, reflux, (ii) POCl_3 , oil bath, 90–100 °C for 6–9 h; (ii) Aryl isothiocyanate derivatives, DMF, reflux, 18–20 h, (iv) PhCOCH_2Br , EtOH, K_2CO_3 .

2.2 Biological Assessment

2.2.1 In Vitro Cytotoxicity of Indole-1,2,4-Triazole Congeners

The cytotoxic activity of the synthesized indole-1,2,4-triazole derivatives (**3–8**) is evaluated using the lactate dehydrogenase (LDH) assay against a panel of human cancer cell lines: MCF-7 (breast adenocarcinoma), HCT-116 (colorectal carcinoma), and HepG2 (hepatocellular carcinoma). Normal BJ-1 human fibroblasts serve as a non-malignant control to assess selectivity. Cells are exposed to Synthetic compounds for 48 h, and viability is measured based on LDH release. Results show that all compounds inhibit growth in the cancer cell lines (HCT-116, HepG2, and MCF-7) in a dose-dependent manner after 48 h exposure, as illustrated in **Figs. 2–4**. Remarkably, most compounds display limited cytotoxic effects on BJ-1 fibroblasts, indicating a favorable selectivity profile (**Figs. 2–5**). The IC_{50} values of the most active derivatives are summarized in **Table 1**. Notably, compounds **3a–3d**, **5**, **6b**, and **6c–8b** exhibit potent antiproliferative activity against MCF-7 cells, with IC_{50} values ranging from 2.3 to 4.8 μM , surpassing the activity of the reference drug doxorubicin ($\text{IC}_{50} = 5.6 \mu\text{M}$) (**Fig. 2, Table 1**).

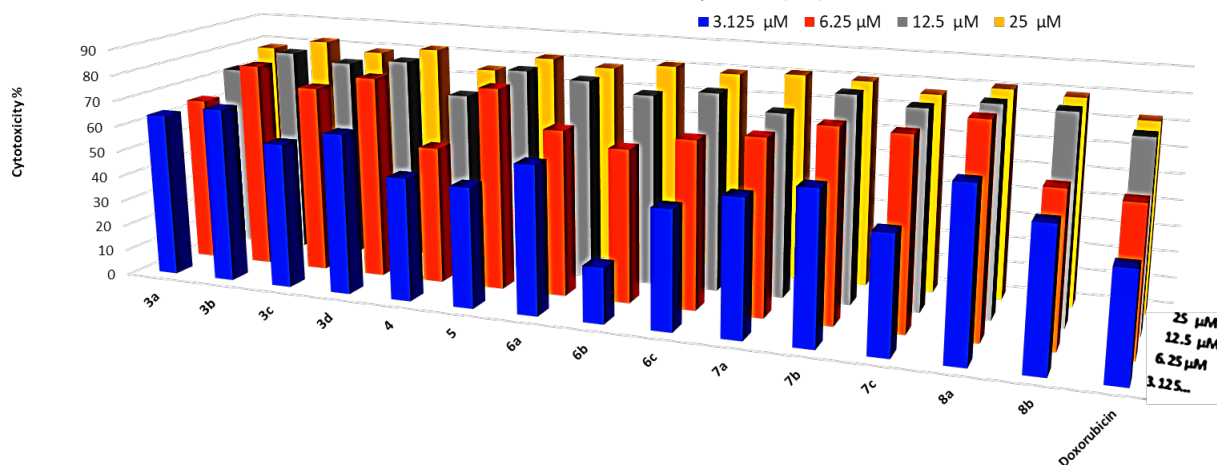


Fig. 2. Dose-dependent antiproliferative data of the fifteen compounds on MCF-7 cancer cells according to the LDH assay after 48 h of exposure.

Against HCT-116 cells, compounds **3b–3d** and **5–8** also show strong activity, with IC_{50} values between 2.6 and 3.1 μM , outperforming doxorubicin ($IC_{50} = 6.5 \mu\text{M}$) by approximately two times. Compounds **1** and **4** show comparable activity to doxorubicin, with IC_{50} values of 6.7 and 5.9 μM , respectively (Fig. 3, Table 1).

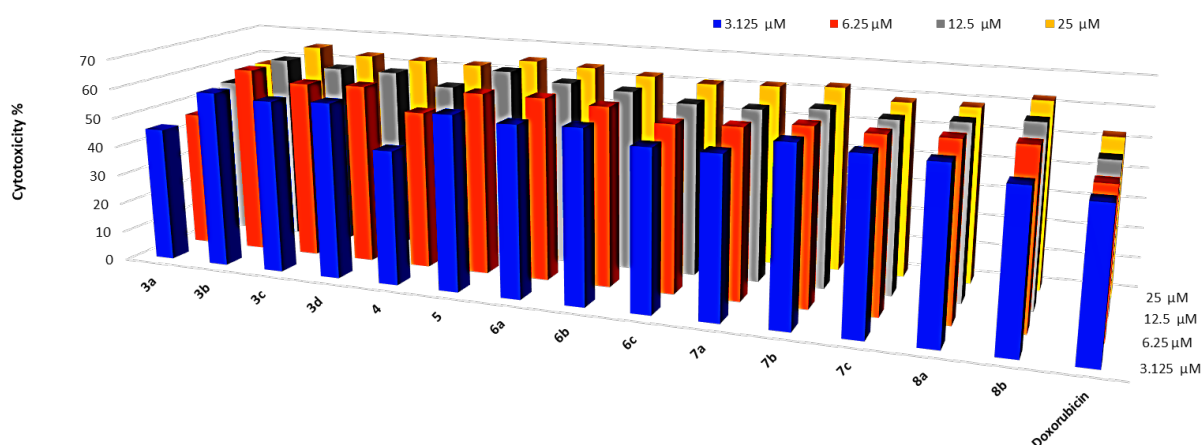


Fig. 3. Dose-dependent antiproliferative data of the fifteen compounds on HCT-116 cancer cells according to the LDH assay after 48 h of exposure.

In HepG2 cells, compounds **3a** and **8a** demonstrate measurable activity ($IC_{50} = 5.9$ and $6.3 \mu\text{M}$, respectively), close to doxorubicin's IC_{50} of $5.6 \mu\text{M}$ (Fig. 4, Table 1).

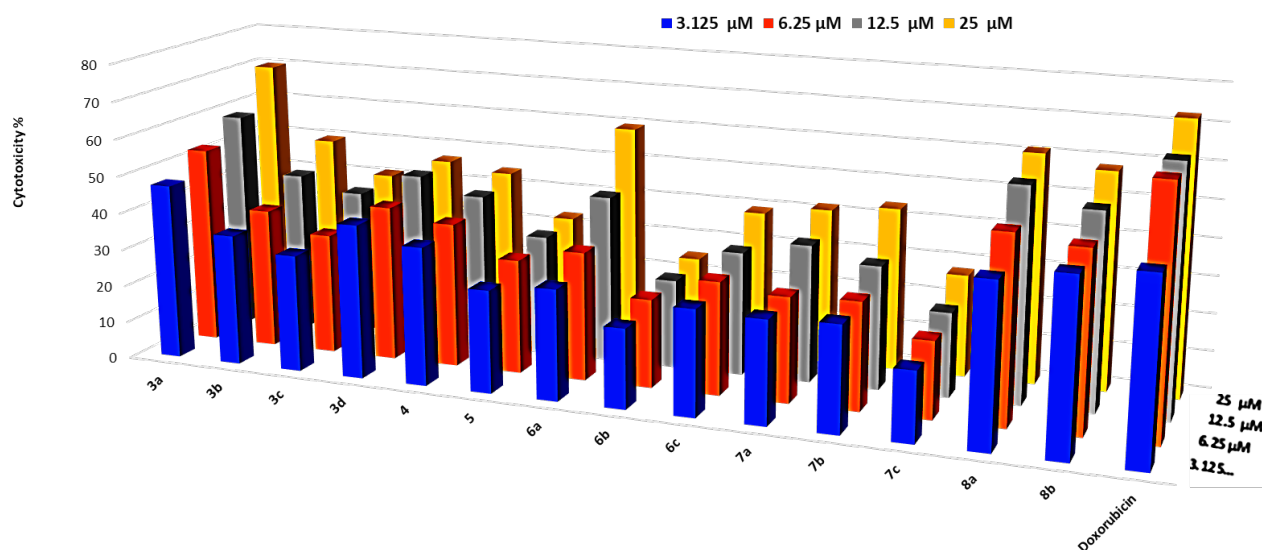


Fig. 4. Dose-dependent antiproliferative data of the fifteen compounds on HepG2 cancer cells according to the LDH assay after 48 h of exposure.

Overall, the indole-1,2,4-triazole hybrids display promising cytotoxic effects, especially against breast and colorectal cancer cell lines. Their relatively lower impact on normal BJ-1 cells supports their potential as selective anticancer agents (Fig. 5).

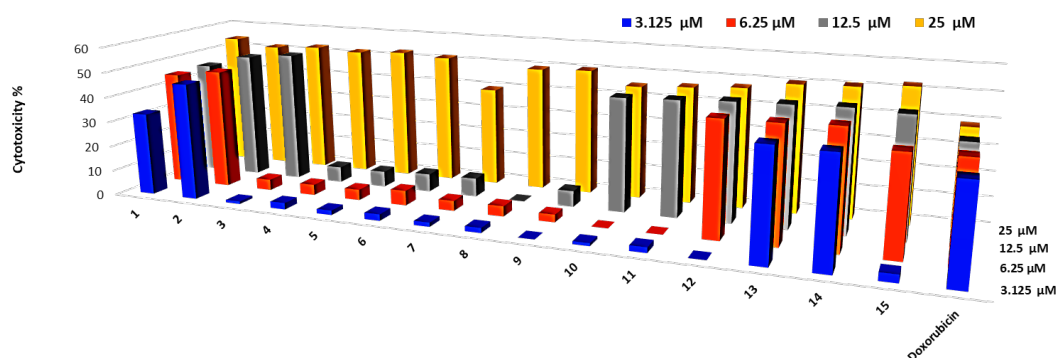


Fig. 5. Dose-dependent antiproliferative data of the fifteen compounds on BJ-1 normal cells according to the LDH assay after 48 h of exposure.

Table 1. Antiproliferative IC_{50} values ($\mu\text{M} \pm \text{SD}$) of the synthesized compounds and doxorubicin against cancer and normal cell lines using the LDH assay.

Compound	IC_{50} (μM) \pm SD			
	MCF-7	HCT-116	HepG2	BJ-1
3a	2.4 \pm 0.1	6.7 \pm 0.2	5.9 \pm 0.2	23.0 \pm 2.1
3b	2.3 \pm 0.1	2.6 \pm 0.1	25.1 \pm 2.2	23.7 \pm 1.9
3c	2.8 \pm 0.2	2.7 \pm 0.1	30.5 \pm 3.1	24.1 \pm 2.1
3d	2.5 \pm 0.2	2.6 \pm 0.1	26.9 \pm 2.3	24.2 \pm 1.8
4	5.9 \pm 0.3	5.9 \pm 0.3	28.1 \pm 2.9	23.9 \pm 1.9
5	4.0 \pm 0.3	2.7 \pm 0.2	37.7 \pm 2.9	23.7 \pm 2.3
6a	5.3 \pm 0.3	2.7 \pm 0.1	50.0 \pm 3.9	31.6 \pm 3.1
6b	2.7 \pm 0.1	2.7 \pm 0.1	14.0 \pm 1.1	24.2 \pm 2.5
6c	4.8 \pm 0.2	2.9 \pm 0.2	31.8 \pm 2.5	25.3 \pm 2.2
7a	3.0 \pm 0.1	3.0 \pm 0.2	30.0 \pm 2.5	24.9 \pm 2.5
7b	4.3 \pm 0.3	2.8 \pm 0.2	45.6 \pm 3.8	27.7 \pm 2.7
7c	2.7 \pm 0.1	2.7 \pm 0.1	28.7 \pm 2.3	27.0 \pm 2.1
8a	2.4 \pm 0.1	2.8 \pm 0.1	6.3 \pm 0.3	24.9 \pm 2.5
8b	3.0 \pm 0.1	3.1 \pm 0.3	12.0 \pm 1.1	24.6 \pm 2.1
Doxorubicin	5.6 \pm 0.3	6.5 \pm 0.5	4.8 \pm 0.5	32.1 \pm 3.1

2.2.2 In Vitro Suppression of Phosphorylated ERK (pERK) in MCF-7 Cells

To explore the mechanism of action, the most active compounds (**3a**, **3b**, **3d**, **5**, **6b**, and **8a**) are tested for their effect on phosphorylated ERK (pERK) levels in MCF-7 cells.⁸ Cells are treated at their IC_{50} concentrations for 24 h. Untreated controls show elevated basal pERK levels (14.16 ± 0.07 pg/mL), reflecting ERK pathway hyperactivation. All compounds significantly reduce pERK levels compared to controls (Fig. 6, Table 2).

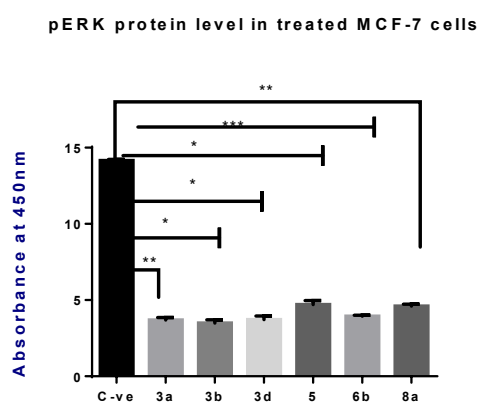


Fig. 6. Effect of compounds **3a**, **3b**, **3d**, **5**, **6b**, and **8a** on pERK protein levels in MCF-7 cells after 24 h incubation at IC_{50} concentrations. Protein levels are measured by quantitative sandwich ELISA and expressed as mean \pm SD ($n = 2$). Statistical significance is determined by one-way ANOVA with multiple comparisons (* $p < 0.05$, ** $p < 0.01$, *** $p < 0.001$, **** $p < 0.0001$ vs. untreated control).

Compound **3b** induces the greatest reduction, lowering pERK to 3.499 ± 0.21 pg/mL, consistent with its potent cytotoxicity. Compounds **3a** and **3d** also strongly inhibit pERK, while **5** and **8a** cause moderate decreases. A clear correlation exists between pERK levels and IC₅₀ values: stronger pERK inhibition corresponds to lower IC₅₀ and higher potency. Compound **3b** exhibits both the lowest pERK and IC₅₀ (2.3 μg/mL), while compound **5** has the highest pERK (4.704 pg/mL) and IC₅₀ (4.0 μg/mL), supporting this relationship.

Table 2. pERK protein levels (pg/mL ± SD) in MCF-7 cells after treatment at IC₅₀ concentrations.

Compound ^a	pERK protein level (pg/mL)
C-ve (untreated cells)	14.16±0.07
3a	3.694±0.16
3b	3.499±0.21
3d	3.723±0.24
5	4.704±0.27
6b	3.938±0.07
8a	4.604±0.13

a: MCF-7cancer cell lines were incubated with IC₅₀ concentration of the tested compounds for 24 h cells.

2.3 In Silico Insights

2.3.1 Molecular Docking Studies on ERK Kinase

To clarify the inhibitory mechanisms of the indole–1,2,4-triazole derivatives, molecular docking simulations characterize their binding interactions with the ERK kinase active site (PDB ID: 5KE0). Compounds **3a**, **3b**, and **3d** are selected for detailed docking using PyRx with AutoDock Vina (version 8). The docking protocol is validated by re-docking the native ligand **6S9**, producing an RMSD of 0 Å, confirming accuracy (Fig. 7A).

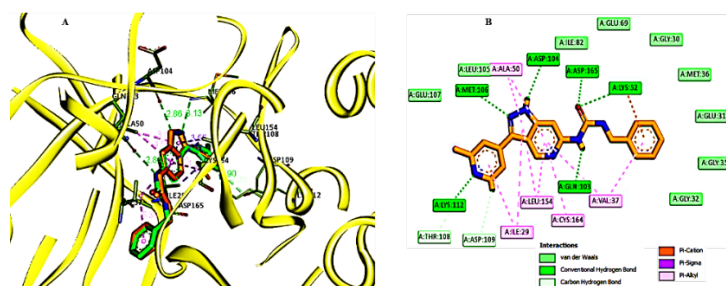


Fig. 7. (A) Superimposed 3D conformations of native (green) and re-docked ligand (brown) within ERK binding pocket (PDB ID: 5KE0); (B) 2D conformation of re-docked ligand **6S9** within ERK binding pocket.

Docking scores show strong binding affinities from -9.0 to -9.7 kcal/mol, closely matching the reference ligand **6S9** (-10.1 kcal/mol) (Table 3). Ligands stably fit within the catalytic cleft, engaging key residues through hydrogen bonds, hydrophobic interactions, and π - π stacking.

The reference ligand **6S9** forms hydrogen bonds with Asp165, Lys52, Gln103, Met106, and Lys112, and hydrophobic contacts with Leu248, Ala250, Lys352, Ala316, Asp109, Thr108, Ile29, Leu154, Cys164, and Val37 (Fig. 7B, Table 3). Compound **3a** exhibits extensive hydrogen bonding and hydrophobic interactions with Asp165, Tyr34, Lys52, Ile54, Leu154, Ala50, Leu105, Arg65, Glu69, Gly165, Ala33, Gly32, Gly35, Met36, Gln103, Asp104, Met106, and Ile29 (Fig. 8, Table 3).

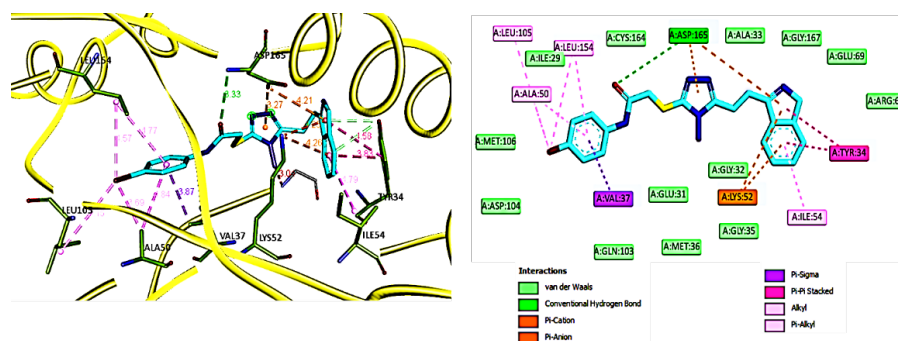


Fig. 8. 3D and 2D binding interactions of compound **3a** within ERK active pocket.

Compound **3b**, the most potent inhibitor, forms three hydrogen bonds with Cys164, Ser151, and Asp16. It also establishes hydrophobic interactions including carbon-hydrogen bonds, π -type interactions, and van der Waals contacts with Gly32, Tyr34, Ile54, Ile29, Val37, Ala50, Leu154, Lys52, Lys149, Asn152, Met106, Leu105, Asp104, Glu31, and Gly35 (Fig. 9, Table 3).

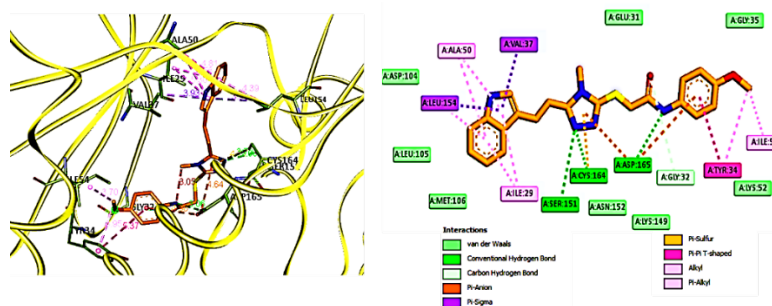


Fig. 9. 3D and 2D binding interactions of compound **3b** within ERK active pocket.

Compound **3d** shows hydrogen bonding with Asp165 and Asn152, along with diverse hydrophobic contacts (Fig. 10, Table 3).

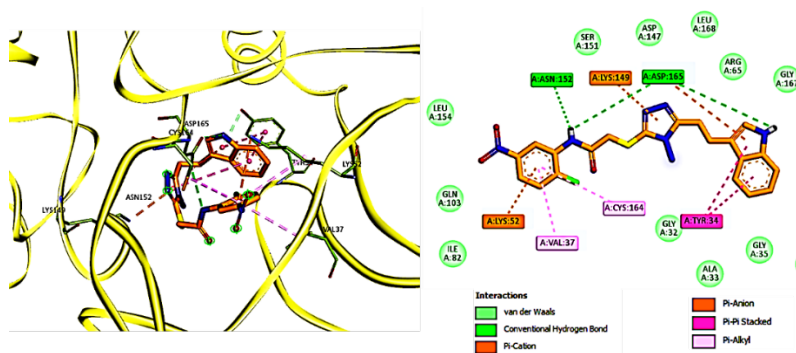


Fig. 10. 3D and 2D binding interactions of compound **3d** within ERK active pocket.

Table 3. Binding affinities and key interactions of compounds **3a**, **3b**, and **3d** with ERK kinase (PDB ID: 5KE0).

Compound	Score Kcal/mol	Moieties from the compound	Amino acid residues	Type of interaction, Distance Å
Ligand 6S9	-10.1	CO, N, NH methylpyridine, pyrazolopyridine, phenyl moieties	Lys52, Asp165, Gln103, Met106, Lys112 Asp109, Thr108, Ile29, Leu154, Cys164, Val37, Ala50, Lys52 Gly32, Gly35, Glu31, Met36, Gly30, Glu69, Ile82, Glu107	Conventional H-bond, 3.13, 2.86, 2.84, 2.90 Carbon H-bond, π -alkyl, π -cation Van der Waals
3a	-9.4	CO Indole and triazole rings Phenyl rings, bromine	Asp165 Tyr34, Asp165, Lys52 Ile54, Leu154, Ala50, Leu105 Arg65, Glu69, Gly165, Ala33, Gly32, Gly35, Met36, Gln103, Asp104, Met106, Ile29	Conventional H-bond, 3.33 Pi-pi stacked, π -anion, π -cation Alkyl, π -alkyl, π -sigma Van der waals
3b	-9.0	N of triazole ring and NH CO, triazole and phenyl rings OCH ₃ , indole moiety	Cys164, Ser151, Asp16 Gly32, Tyr34 Ile54, Ile29, Val37, Ala50, Leu154 Aly52, Lys149, Asn152, Met106, Leu105, Asp104, Glu31, Gly35	Conventional H-bond, 3.06, 3.79, 2.90 Carbon H-bond, π -anion, π -sulfur, pi-sigma, π - π T-shaped Alkyl, π -alkyl Van der Waals
3d	-9.4	NH groups Indole, triazole and phenyl moieties	Asp165, Asn152 Tyr34, Lys149, Lys52, ASP165, Cys164, Val37 Ile54, Gly35, Ala33, Gly32, Ile82, Gln103, Leu154, Ser151, Asp147, Leu168, Arg65, Gly167	Conventional H-bond, 3.15, 3.27 π - π Stacked, π -cation, π -anion, π -alkyl Van der Waals

2.3.2 Drug-Likeliness and ADMET Profiling

The pharmacokinetic and drug-likeness profiles of compounds **3a**, **3b**, and **3d** are evaluated using the SwissADME platform (<http://www.swissadme.ch/index.php>), benchmarked against doxorubicin. Evaluations follow Lipinski's Rule of Five and Veber's criteria, detailed in Table 4.^{32,33} All compounds conform well to drug-likeness except 3d, which exceeds the recommended topological polar surface area (TPSA), similar to doxorubicin.

Table 4. Drug-likeness and key physicochemical properties of compounds **3a**, **3b**, and **3d** as predicted by SwissADME.

Compound	MWt g/mol	Log P	HBA	HBD	TPSA Å ²	Fraction Csp3	MR	nRB	Drug-likeness	
									No. Lipinski violation	No. Veber violation
3a	471.37	2.99	3	3	126.92	0.15	119.54	8	0	0
3b	422.50	2.09	4	3	136.15	0.19	118.33	9	0	0
3d	471.92	2.03	5	3	172.74	0.15	125.67	9	0	1
Doxorubicin	543.52	-2.1	12	6	206.07	0.44	132.66	5	3	1

MWt: Molecular weight; Log P: lipophilicity (log octanol/water partition coefficient); HBA: Hydrogen bond acceptor; HBD: Hydrogen bond donor; TPSA: Topological polar surface area; MR: Molar reactivity; nRB: number of rotatable bonds.

Compound **3b** demonstrates optimal physicochemical properties within the bioavailability radar, covering lipophilicity, molecular size, polarity, solubility, and flexibility, with only a minor deviation in the unsaturation parameter (**Fig. 11**). In contrast, compounds **3a**, **3d**, and doxorubicin show deviations in one or more parameters such as saturation and polarity.

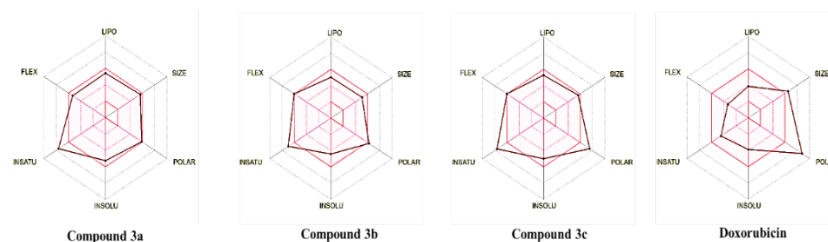


Fig. 11. Bioavailability radar chart of the most active compounds **3a**, **3b**, **3d**, and doxorubicin. The ideal range for each oral bioavailability factor is represented by the pink region, while the red lines indicate the measured values of the evaluated compounds. The colored zone defines the typical physicochemical space for oral bioavailability. Parameters include: LIPO (lipophilicity) with $-0.7 < \text{XLOGP3} < +5$; SIZE (molecular weight) between 150 and 500 g/mol; POLAR (polarity) with TPSA between 20 and 130 Å²; INSOLU (insolubility) with log S between -6 and 0; INSATU (unsaturation) with Fraction Csp3 between 0.25 and 1; and FLEX (flexibility) with the number of rotatable bonds between 0 and 9.

Table 5. Predicted ADMET parameters of compounds **3a**, **3b**, and **3d** based on *pkCSM* computational analysis.

Parameters* (unite)	3a	3b	3d	Doxorubicin
Absorption				
Water solubility (log mol/L)	-3.859	-3.866	-3.84	-3.20
Caco2 permeability (log Papp in 10 ⁻⁶ cm/s)	0.204	0.288	-0.637	0.403
Intestinal absorption (human)	87.031	82.458	84.016	62.63
Skin Permeability (log Kp)	-2.763	-2.756	-2.738	-2.73
P-glycoprotein substrate	Yes	Yes	Yes	Yes
P-glycoprotein I inhibitor	Yes	Yes	Yes	No
P-glycoprotein II inhibitor	Yes	Yes	Yes	No
Distribution				
VDss (human) (log L/kg)	-0.173	-0.104	-0.246	1.07
Blood-Brain Barrier (log BB)	-1.199	-1.207	-1.378	-1.559
CNS permeability (log PS)	-2.367	-2.67	-2.609	-4.366
Metabolism				
CYP2D6 substrate	No	No	No	No
CYP3A4 substrate	Yes	Yes	Yes	No
CYP1A2 inhibitor	Yes	Yes	Yes	No
CYP2C19 inhibitor	Yes	Yes	Yes	No
CYP2C9 inhibitor	Yes	Yes	Yes	No
CYP2D6 inhibitor	No	No	No	No
CYP3A4 inhibitor	Yes	Yes	Yes	No
Excretion				
Total Clearance (log ml/min/kg)	-0.175	0.015	0.193	0.817
Renal OCT2 substrate	No	No	No	No
Toxicity				
Ames mutagenicity	Yes	Yes	Yes	Yes
Max. tolerated dose (human)(log mg/kg/day)	0.604	0.565	0.393	0.488
hERG I inhibitor	No	No	No	No
hERG II inhibitor	Yes	Yes	Yes	Yes
Oral Rat Acute Toxicity (LD50, mol/kg)	2.729	2.708	2.685	3.693
Oral Rat Chronic Toxicity (log mg/kg_bw/day)	2.082	1.943	2.719	2.659
Hepatotoxicity	Yes	Yes	Yes	No
Skin Sensitization	No	No	No	No
T.Pyriformis toxicit (log ug/L)	0.323	0.311	0.292	0.285
Minnow toxicity (log mM)	-0.725	-0.177	-1.712	7.57

*Solubility classification based on log S: very soluble (> 0), extremely soluble (-2 to 0), soluble (-4 to -2), moderately soluble (-6 to -4), weakly soluble (-10 to -6), insoluble (< -10). High Caco-2 permeability indicated by log Papp > 0.9; low skin permeability by log Kp > -2.5. Volume of distribution (VDss) is low if log VDss < -0.15, high if log VDss > 0.45. Compounds with log BB > 0.3 readily cross the blood-brain barrier; those with log BB < -1 poorly distribute to the brain. CNS penetration expected if log PS > -2, unlikely if < -3.

Recognizing the critical importance of safety in drug development,³⁴ *in silico* ADMET properties were predicted using the *pkCSM* server (<http://biosig.unimelb.edu.au/pkcsml/>) to evaluate absorption, distribution, metabolism, excretion, and toxicity, summarized in **Table 5**. The compounds exhibit moderate aqueous solubility ($\log S \sim -3.8$), comparable to doxorubicin. Intestinal absorption is notably higher (>82%) compared to doxorubicin (62.63%), though Caco-2 permeability and volume of distribution are lower. All compounds act as substrates and inhibitors of P-glycoprotein I/II, differing from doxorubicin's profile. Predicted blood–brain barrier penetration and CNS permeability are low ($\log BB < -1$ and $\log PS < -2$), indicating limited central nervous system exposure. Cytochrome P450 enzymes are key detoxification catalysts metabolizing many drugs.³⁵ The compounds are substrates of CYP3A4 but not CYP2D6, and inhibit CYP1A2, CYP2C19, CYP2C9, and CYP3A4 isoforms, suggesting potential drug–drug interactions absent in doxorubicin. Excretion is mainly assessed by total clearance, reflecting hepatic and renal elimination affecting bioavailability. Among tested compounds, **3d** shows the highest predicted clearance, yet all are lower than doxorubicin. The OCT2 transporter mediates renal drug uptake; its inhibition can cause drug accumulation and nephrotoxicity.^{35,36} None of the compounds are predicted to inhibit OCT2, suggesting lower kidney toxicity risk. Toxicity predictions reveal all compounds and doxorubicin are Ames mutagenic. Compounds **3a**, **3b**, and **3d** inhibit hERG II but not hERG I channels, indicating possible cardiac safety risks. Hepatotoxicity is predicted for all test compounds but not for doxorubicin. Acute oral toxicity (LD_{50}) is lower than doxorubicin, with **3b** showing the lowest chronic toxicity potential. None are predicted to cause skin sensitization.

3. Conclusions

A new series of indole–1,2,4-triazole hybrids was synthesized and systematically investigated for their anticancer properties. Several derivatives exhibited potent and selective cytotoxicity against MCF-7 and HCT-116 cell lines with minimal impact on normal fibroblasts. Among them, compound **3b** demonstrated superior efficacy, characterized by the lowest IC_{50} (2.3 μM) and most pronounced suppression of phosphorylated ERK levels (3.499 pg/mL). Its optimized structural features—particularly the indole core and 4-methoxyphenyl-acetamide moiety—facilitated high-affinity binding to the ERK active site through key hydrogen bonding and hydrophobic interactions, as confirmed by molecular docking. Complementary *in silico* ADMET profiling further validated its favorable drug-likeness and pharmacokinetics. Collectively, these results highlight compound **3b** as a compelling lead for selective ERK-targeted anticancer drug development, meriting further *in vivo* evaluation and structure-based optimization.

4. Experimental

4.1 Materials and Methods

All solvents and reagents were of analytical grade and used as received. Indole-3-propionic acid was purchased from Sigma-Aldrich. Melting points were recorded on an Electrothermal 9100 digital melting point apparatus and are uncorrected. Reaction progress was monitored by thin-layer chromatography (TLC) on silica gel plates and visualized under UV light at 254 nm. Infrared (IR) spectra were recorded on a Bruker-5000 FT-IR spectrometer. ^1H and ^{13}C NMR spectra were obtained on a JEOL-ECA-500 NMR spectrometer operating at 500 and 125 MHz, respectively, using tetramethylsilane (TMS) as the internal standard, at the National Research Center, Egypt. Proton coupling patterns are designated as singlet (s), doublet (d), triplet (t), quartet (q), and multiplet (m). Chemical shifts are reported in parts per million (ppm) relative to the solvent peak. Electron ionization mass spectra (EI-MS) were acquired on a Finnigan Mat SSQ 7000 system operating at 70 eV (Thermo Inst. Sys. Inc., USA). The synthesis of 5-(2-(1*H*-indol-3-yl)ethyl)-4-amino-4*H*-1,2,4-triazole-3-thiol and 2-chloro-*N*-(substituted phenyl)acetamides was conducted according to previously reported methods.^{37–39}

4.2 Chemistry

4.2.1 Synthesis of 5-(2-(1*H*-indol-3-yl)ethyl)-4-amino-4*H*-1,2,4-triazole-3-thiol (**2**)

A mixture of 3-(1*H*-indol-3-yl)propanoic acid (**1**, 0.01 mol) and thiocarbonylhydrazide (0.01 mol) was heated at 130 °C for 5 h in an oil bath. After cooling, a 20% aqueous solution of sodium carbonate (Na_2CO_3 , 10 mL) was added, and the mixture was heated for an additional 30 minutes at 70 °C. Upon cooling, the precipitate was filtered, washed with water, air-dried, and recrystallized from methanol.

Brown solid; m.p: 154–156 °C; yield: 80%; ^1H NMR (500 MHz, $\text{DMSO}-d_6$) δ (ppm): 13.43 (s, 1H, SH), 10.79 (s, 1H, NH), 7.51 (d, $J = 4.5$ Hz, 1H, indolyl, H-4), 7.30 (d, $J = 3.8$ Hz, 1H, indolyl, H-7), 7.13 (d, $J = 2.0$ Hz, 1H, indolyl, H-2), 7.04–6.94 (dd, $J = 3.7, 2.9$ Hz, 2H, indolyl, H-6&7), 5.66 (s, 2H, NH_2), 3.83 (s, 2H, CH_2), 3.05–2.95 (m, 4H, $\text{CH}_2\text{-CH}_2$).

4.2.2 General procedure for the preparation of 2-((5-(2-(1*H*-indol-3-yl)ethyl)-4-amino-4*H*-1,2,4-triazol-3-yl)thio)-*N*-(substituted phenyl)acetamides (**3a–d**)

A mixture of compound **2** (0.01 mol) and the corresponding 2-chloro-*N*-(substituted phenyl)acetamide (0.01 mol) was refluxed in 20 mL of dimethylformamide (DMF) containing triethylamine (0.02 mol) for 14–16 h, monitored by TLC. After completion, the reaction mixture cooled and poured into ice-cold water. The resulting precipitate was filtered, washed with water, dried, and recrystallized from a mixture of *n*-hexane and ethyl acetate (3:1).

4.2.2.1 2-((5-(2-(1*H*-indol-3-yl)ethyl)-4-amino-4*H*-1,2,4-triazol-3-yl)thio)-*N*-(4-bromophenyl) acetamide (**3a**)

Pale brown solid; m.p: 129-31 °C; yield: 56%; IR (KBr) cm^{-1} : 3404 (NH₂), 3250 (NH), 1702 (C=O), 1618 (C=N), 1573 (C=C); ¹H NMR (500 MHz, DMSO-*d*₆) δ (ppm): 10.77, 10.10 (2s, 2H, NH), 7.55-6.84 (m, 9H, Ar-H), 6.03 (s, 2H, NH₂), 3.83 (s, 2H, CH₂), 3.03-3.01 (m, 4H, CH₂-CH₂); ¹³C NMR (125 MHz, DMSO-*d*₆) δ (ppm): 168.75 (C=O), 154.39 (S-C=N), 141.46 (C=N), 129.54, 128.09, 122.81, 121.47, 119.62, 118.81, 118.74, 113.85, 112.16, 111.87, 38.36 (S-CH₂), 25.45 (CH₂), 23.14 (CH₂); EIMS, *m/z*: 470/472 (M⁺/M⁺+2) for C₂₀H₁₉N₆OS (471.38).

4.2.2.2 2-((5-(2-(1*H*-indol-3-yl)ethyl)-4-amino-4*H*-1,2,4-triazol-3-yl)thio)-*N*-(4-methoxyphenyl) acetamide (**3b**)

Brown solid; m.p: 175-177 °C; yield: 55 %; IR (KBr) cm^{-1} : 3359 (NH₂), 3262, 3165 (NH), 1660 (C=O), 1605 (C=N), 1549 (C=C), 1234, 1171 (C-O); ¹H NMR (500 MHz, DMSO-*d*₆) δ (ppm): 10.78, 10.20 (2s, 2H, 2NH), 7.59-7.44 (m, 3H, Ar-H), 7.32 (m, 2H, Ar-H), 7.05 (d, 1H, Ar-H), 6.86-6.84 (m, 3H, Ar-H), 5.93 (s, 2H, NH₂), 4.01 (s, 2H, CH₂), 3.69 (s, 3H, OCH₃), 3.03-3.01 (m, 4H, CH₂-CH₂); ¹³C NMR (125 MHz, DMSO-*d*₆) δ (ppm): 164.60 (C=O), 151.40 (C=N), 136.74, 131.07, 127.40, 125.10, 123.15, 121.48, 118.51, 115.17, 115.07, 113.20, 111.94, 90.89, 56.76 (OCH₃), 44.01 (S-CH₂), 26.50 (CH₂), 22.36 (CH₂); EIMS, *m/z*: 422 (M⁺) for C₂₁H₂₂N₆O₂S.

4.2.2.3 2-((5-(2-(1*H*-indol-3-yl)ethyl)-4-amino-4*H*-1,2,4-triazol-3-yl)thio)-*N*-(4-nitrophenyl) acetamide (**3c**)

Dark brown solid; m.p: 220-222 °C; yield: 57 % for C₂₀H₁₉N₇O₃S (437.48); IR (KBr) cm^{-1} : 3342 (NH₂), 3292, 3154 (NH), 1697 (C=O), 1612 (C=N), 1597 (C=C); ¹H NMR (500 MHz, DMSO-*d*₆) δ (ppm): 10.75 (s, 2H, NH), 8.21 (d, 2H, p-nitrophenyl H-3 & 5), 8.00-7.83 (m, 3H, p-nitrophenyl H-2, -6 & indolyl H-4), 7.54 (m, 1H, indolyl H-7), 7.29 (d, 1H, indolyl H-2), 7.03 (m, 1H, indolyl H-5), 6.68 (m, 1H, indolyl H-6), 5.68 (s, 2H, NH₂), 4.13 (s, 2H, CH₂), 3.10-3.05 (m, 4H, CH₂-CH₂); ¹³C NMR (125 MHz, DMSO-*d*₆) δ (ppm): 167.45 (C=O), 156.50 (C=N), 137.00, 136.30, 132.02, 121.70, 119.62, 118.87, 114.55, 114.07, 113.93, 113.88, 112.24, 112.18, 111.92, 110.98, 44.00 (S-CH₂), 24.92 (CH₂), 23.36 (CH₂).

4.2.2.4 2-((5-(2-(1*H*-indol-3-yl)ethyl)-4-amino-4*H*-1,2,4-triazol-3-yl)thio)-*N*-(2-chloro-5-nitrophenyl) acetamide (**3d**)

Brown solid; m.p: 225-227 °C; yield: 59 %; IR (KBr) cm^{-1} : 3349, 3334 (NH₂), 3176 (NH), 1692 (C=O), 1618 (C=N), 1594 (C=C), ¹H NMR (500 MHz, DMSO-*d*₆) δ (ppm): 10.79, 10.76 (2s, 2H, NH), 8.51 (d, 1H, phenyl H-6), 7.92-6.94 (m, 7H, phenyl & indolyl H), 5.85 (s, 2H, NH₂), 3.31 (s, 2H, CH₂), 3.04, 2.85 (m, 4H, CH₂-CH₂); EIMS, *m/z*: 471/473 (M⁺/M⁺+2) for C₂₀H₁₈ClN₇O₃S (471.92).

4.2.3 Synthesis of 5,5'-(ethane-1,2-diylbis(sulfanediy))bis(3-(2-(1*H*-indol-3-yl)ethyl)-4*H*-1,2,4-triazol-4-amine) (**4**)

A mixture of compound **2** (0.02 mol) and 1,2-dibromoethane (0.01 mol) in dry acetone (10 mL) containing anhydrous potassium carbonate (0.02 mol) was refluxed for 12 h under stirring until completion (monitored by TLC). The reaction mixture was cooled, poured into ice, and the precipitate was filtered, washed with water, air-dried, and recrystallized from *n*-hexane/ethyl acetate.

Light brown solid; m.p: 218-220 °C; yield 64 % for C₂₆H₂₈N₁₀S₂ (544.70); IR (KBr) cm^{-1} : 3499, 3394, 3334, 3279 (NH₂) 3176, 3055 (NH), 1692, 1618 (C=N), 1594 (C=C); ¹H NMR (500 MHz, DMSO-*d*₆) δ (ppm): 10.78 (s, 2H, 2NH), 7.54-7.50 (m, 2H, indolyl H-4 & 4'), 7.32 (s, 2H, indolyl, H-7 & 7'), 7.16-6.95 (m, 6H, bisindolyl H-2, -5 & 6), 5.90 (s, 2H, NH₂), 5.32 (s, 2H, NH₂), 3.91-2.65 (m, 12H, 3CH₂-CH₂); ¹³C NMR (125 MHz, DMSO-*d*₆) δ (ppm): 171.33, 156.84, 153.65 & 150.93 (S-C=N), 148.23, 136.80, 127.52, 123.02, 122.84, 121.49, 118.78, 114.07, 111.93, 31.61 (S-CH₂), 26.48 (S-CH₂), 25.59, 25.23, 22.81 (CH₂), 22.25 (CH₂).

4.2.4 Synthesis of 3-(2-(1*H*-indol-3-yl)ethyl)-[1,2,4]triazolo[3,4-*b*][1,3,4]thiadiazole-6-thiol (**5**)

A mixture of 5-(2-(1*H*-indol-3-yl)ethyl)-4-amino-4*H*-1,2,4-triazole-3-thiol (**2**, 0.01 mol), carbon disulfide (20 mL), and potassium hydroxide (5.6 g, 0.01 mol) in methanol (50 mL) was refluxed with continuous stirring for 24 h. Upon completion of the reaction (monitored by TLC), the solvent was removed under reduced pressure, and the residue was poured into 200 mL of water. The solution was acidified with 5% aqueous HCl until reaching an acidic pH (verified by pH paper), resulting in the formation of a white precipitate. The solid was filtered, washed, air-dried, and obtained as a highly pure compound without the need for further purification.

Off-white solid; m.p: 215-217 °C; yield: 84 %; IR (KBr) cm^{-1} : 3265 (NH), 2693 (SH), 1617 (C=N), 1560 (C=C); ¹H NMR (500 MHz, DMSO-*d*₆) δ (ppm): 12.50 (s, 1H, SH), 10.84 (s, 1H, NH), 7.43 (d, 1H, indolyl H-4), 7.31 (d, 1H, indolyl H-7), 7.14 -6.94 (m, 3H, indolyl H-2, -5 & 6), 3.31-3.30 (m, 4H, CH₂-CH₂); ¹³C NMR (125 MHz, DMSO-*d*₆) δ (ppm): 184.17 (N=C-SH), 167.69 (S-C=N), 162.38 (N-C=N), 136.22, 126.96, 122.43, 120.93, 118.22, 113.36, 111.38, 25.15 (CH₂), 24.69 (CH₂); EIMS, *m/z*: 301 (M⁺) for C₁₃H₁₁N₅S₂ (301.39).

4.2.5 General procedure for synthesizing of 3-(2-(1*H*-indol-3-yl)ethyl)-6-(substituted phenyl)-[1,2,4] triazolo[3,4-*b*][1,3,4]thiadiazoles (**6a-c**)

A mixture of 5-(2-(1*H*-indol-3-yl)ethyl)-4-amino-4*H*-1,2,4-triazole-3-thiol (**2**, 0.01 mol) and 2-chloro or 4-nitro benzoic acids or 2,4-dinitro benzoyl chloride (0.01 mol) was heated in freshly distilled phosphorus oxychloride (POCl₃, 4 mL) at 90–100 °C

for 6–9 h in an oil bath. After cooling, the reaction mixture was added dropwise under vigorous stirring into an aqueous sodium bicarbonate solution (NaHCO₃, 0.001 mol in 20 mL water). The resulting solid was collected by filtration, washed with water, air-dried, and recrystallized from methanol.

4.2.5.1 3-(2-(1*H*-indol-3-yl)ethyl)-6-(2-chlorophenyl)-[1,2,4]triazolo[3,4-*b*][1,3,4]thiadiazole (**6a**)

Brown solid, m.p: 292–294 °C; yield: 79 %; IR (KBr) cm⁻¹: 3116 (NH), 1618 (C=N), 1602 (C=C); ¹H NMR (500 MHz, DMSO-*d*₆) δ (ppm): 10.97 (s, 1H, NH), 7.96–7.93 (m, 2H, Ar-H), 7.75–7.53 (m, 5H, Ar-H), 7.33 (d, 1H, Ar-H), 7.06 (m, 1H, Ar-H), 3.07–3.04 (m, 4H, CH₂-CH₂); ¹³C NMR (125 MHz, DMSO-*d*₆) δ (ppm): 168.39, 162.26 & 155.71 (C=N of thiadiazole ring), 148.35, 145.13, 141.60, 138.79, 136.67, 133.15, 132.84, 130.64, 129.22, 125.40, 123.58, 121.85, 120.76, 117.96, 114.80, 110.88, 26.27 (CH₂), 25.53 (CH₂); EIMS, *m/z*: 379/381 (M⁺/M⁺²) for C₁₉H₁₄ClN₅S (379.87).

4.2.5.2 3-(2-(1*H*-indol-3-yl)ethyl)-6-(4-nitrophenyl)-[1,2,4]triazolo[3,4-*b*][1,3,4]thiadiazole (**6b**)

Green solid, m.p: 275–277 °C; yield: 82 % for C₁₉H₁₄N₆O₂S (390.42); IR (KBr) cm⁻¹: 32(NH), (C=N), (C=C); ¹H NMR (500 MHz, DMSO-*d*₆) δ (ppm): 10.78 (s, 1H, NH), 8.97–8.8 (m, 4H, *p*-nitrophenyl-H), 7.24 (d, 1H, indolyl H-4), 7.15–7.14 (m, 2H, indolyl H-7 & 2), 7.00–6.92 (m, 3H, indolyl H-5 & 6), 3.01 (m, 4H, CH₂-CH₂); ¹³C NMR (125 MHz, DMSO-*d*₆) δ (ppm): 164.47, 153.23 & 150.01 (C=N of thiadiazole ring), 147.84, 136.74, 135.11, 128.93, 127.28, 125.12, 124.56, 121.75, 119.15, 118.99, 112.05, 108.38, 26.50 (CH₂), 22.36 (CH₂).

4.2.5.3 3-(2-(1*H*-indol-3-yl)ethyl)-6-(2,4-dinitrophenyl)-[1,2,4]triazolo[3,4-*b*][1,3,4]thiadiazole (**6c**)

Brown solid, m.p: 252–254 °C; yield: 80 % for C₁₉H₁₃N₇O₄S (435.42); IR (KBr) cm⁻¹: 3307 (NH), 1626 (C=N), 1595 (C=C); ¹H NMR (500 MHz, DMSO-*d*₆) δ (ppm): 10.96 (s, 1H, NH), 8.95–8.90 (m, 3H, 2,4-dinitrophenyl-H), 7.63 (d, 1H, indolyl H-4), 7.31 (m, 2H, indolyl H-2 & 7), 7.03–6.97 (m, 2H, indolyl H-5 & 6), 3.01–2.93 (m, 4H, CH₂-CH₂); ¹³C NMR (125 MHz, DMSO-*d*₆) δ (ppm): 171.62, 169.53 & 174.26 (C=N of thiadiazole ring), 136.71, 129.14, 127.28, 124.43, 121.71, 119.08, 119.00, 115.78, 114.14, 112.03, 26.69 (CH₂), 21.53 (CH₂).

4.2.6 General procedure of preparation of 3-(2-(1*H*-indol-3-yl)ethyl)-*N*-(substituted phenyl)-[1,2,4]triazolo[3,4-*b*][1,3,4]thiadiazol-6-amine (**7a-c**)

A mixture of 5-(2-(1*H*-indol-3-yl)ethyl)-4-amino-4*H*-1,2,4-triazole-3-thiol (**2**, 0.01 mol) and various aryl isothiocyanate derivatives, namely phenyl isothiocyanate, 4-methoxy and 4-nitro phenyl isothiocyanates (0.01 mol) was refluxed in dimethylformamide (DMF, 20 mL) with stirring for 18–20 h. Upon completion, the reaction mixture was cooled in an ice bath, and the precipitate was collected by filtration, washed thoroughly with water, air-dried, and recrystallized from a mixture of *n*-hexane and ethyl acetate.

4.2.6.1 3-(2-(1*H*-Indol-3-yl)ethyl)-*N*-phenyl-[1,2,4]triazolo[3,4-*b*][1,3,4]thiadiazol-6-amine (**7a**)

Beige solid; m.p: 172–174 °C; yield: 54 %; IR (KBr) cm⁻¹: 3350, 3214 (NH), 1602 (C=N), 1513 (C=C); ¹H NMR (500 MHz, DMSO-*d*₆) δ (ppm): 10.77 (s, 2H, 2NH), 7.29–6.94 (m, 10H, Ar-H), 3.03–2.84 (m, 4H, CH₂-CH₂); ¹³C NMR (125 MHz, DMSO-*d*₆) δ (ppm): 169.66, 148.19, 138.71, 136.71, 132.07, 131.92, 122.99, 121.75, 121.40, 118.77, 115.45, 114.81, 111.92, 109.60, 107.62, 100.00, 26.48 (CH₂), 22.25(CH₂); EIMS, *m/z*: 360 (M⁺) for C₁₉H₁₆N₆S (360.44).

4.2.6.2 3-(2-(1*H*-Indol-3-yl)ethyl)-*N*-(4-methoxyphenyl)-[1,2,4]triazolo[3,4-*b*][1,3,4]thiadiazol-6-amine (**7b**)

Light yellow solid; m.p: 176–178 °C; yield: 52 % for C₂₀H₁₈N₆OS (390.47); IR (KBr) cm⁻¹: 3285 (NH), 1618 (C=N), 1570 (C=C); ¹H NMR (500 MHz, DMSO-*d*₆) δ (ppm): 10.76 (s, 2H, 2NH), 7.68–7.03 (m, 9H, Ar-H), 3.74 (s, 3H, OCH₃), 3.01, 2.88 (m, 4H, CH₂-CH₂); ¹³C NMR (125 MHz, DMSO-*d*₆) δ (ppm): 162.40, 149.77, 139.00, 138.40, 137.82, 137.52, 129.23, 128.29, 127.94, 127.88, 127.81, 127.55, 119.02, 112.55, 111.80, 110.95, 51.70, 26.05 (CH₂), 24.07 (CH₂).

4.2.6.3 3-(2-(1*H*-indol-3-yl)ethyl)-*N*-(4-nitrophenyl)-[1,2,4]triazolo[3,4-*b*][1,3,4]thiadiazol-6-amine (**7c**)

Brown solid; m.p: 185–187 °C; yield: 51 %; IR (KBr) cm⁻¹: 3291, 3050 (NH), 1616 (C=N), 1574 (C=C); ¹H NMR (500 MHz, DMSO-*d*₆) δ (ppm): 10.77, 10.75 (2s, 2H, NH), 7.92–6.94 (m, 9H, Ar-H), 3.04, 2.93 (m, 4H, CH₂-CH₂); EIMS, *m/z*: (M⁺) for C₁₉H₁₅N₇O₂S (405.44).

4.2.7 General procedure for synthesizing 3-(2-(1*H*-indol-3-yl)ethyl)-6-(4-substituted phenyl)-7*H*-[1,2,4]triazolo[3,4-*b*][1,3,4]thiadiazine (**8a,b**)

To a solution of 5-(2-(1*H*-indol-3-yl)ethyl)-4-amino-4*H*-1,2,4-triazole-3-thiol (**2**, 0.01 mol) in absolute ethanol (10 mL) containing anhydrous potassium carbonate (0.02 mmol), the appropriate 2-bromoacetophenone derivative (0.01 mol) was added. The reaction mixture was refluxed for 4 h (monitored by TLC). After cooling, the precipitate was filtered, washed with water, air-dried, and recrystallized from a mixture of *n*-hexane and ethyl acetate.

4.2.7.1 3-(2-(1*H*-Indol-3-yl)ethyl)-6-phenyl-7*H*-[1,2,4]triazolo[3,4-*b*][1,3,4]thiadiazine (**8a**)

Brown solid; m.p: 174-176 °C; yield: 55 %; IR (KBr) cm^{-1} : 3297 (NH₂), 1618 (C=N), 1596 (C=C); ¹H NMR (500 MHz, DMSO-*d*₆) δ (ppm): 10.77 (s, 1H, NH), 7.91 (s, 1H, indolyl, H-2), 7.29-6.93 (m, 9H, Ar-H), 4.00 (s, 2H, CH₂ of thiadiazine), 3.04-2.71 (m, 4H, CH₂-CH₂); EIMS, *m/z*: 359 (M⁺) for C₂₀H₁₇N₅S (359.45).

4.2.7.2 3-(2-(1*H*-Indol-3-yl)ethyl)-6-(4-bromophenyl)-7*H*-[1,2,4]triazolo[3,4-*b*][1,3,4]thiadiazine (**8b**)

Black solid; m.p: 180-182 °C; yield: 59 %; IR (KBr) cm^{-1} : 3247 (NH), 1619 (C=N), 1590 (C=C); ¹H NMR (500 MHz, DMSO-*d*₆) δ (ppm): 10.76 (s, 1H, NH), 7.57-7.03 (m, 9H, Ar-H), 4.00 (s, 2H, CH₂ of thiadiazine), 3.05 (m, 4H, CH₂-CH₂); EIMS, *m/z*: 437/439 (M⁺/M²⁺) for C₂₀H₁₆BrN₅S (438.35).

4.3 Biological Assessment

4.3.1 Evaluation of the *In vitro* Anti-cancer Efficacy

4.3.1.1 Cell Lines and Culture Conditions

Human cancer cell lines MCF-7 (breast adenocarcinoma), HCT-116 (colorectal carcinoma), and HepG2 (hepatocellular carcinoma), along with normal BJ-1 human fibroblasts, were obtained from the American Type Culture Collection (ATCC). Cells were cultured in Dulbecco's Modified Eagle Medium (DMEM) supplemented with 10% fetal bovine serum (FBS) and 1% penicillin-streptomycin (100 IU/mL and 100 $\mu\text{g}/\text{mL}$, respectively). Cultures were maintained at 37 °C in a humidified incubator with 5% CO₂.

4.3.1.2 *In Vitro* Cytotoxicity Assay

Cytotoxic activity was assessed *via* the lactate dehydrogenase (LDH) release assay.⁴⁰ Cells were seeded in 96-well plates at a density of 5×10^4 cells/well, treated with various concentrations of test compounds, and incubated for 48 h. Doxorubicin served as a positive control. LDH levels in culture supernatants were quantified using a commercial colorimetric assay kit and absorbance measured at 490 nm by a BioTek ELx800 microplate reader. All experiments were independently conducted in triplicate (*n* = 3). Data are expressed as mean \pm standard deviation (SD). Statistical significance among groups and IC₅₀ values were calculated using probit analysis *via* SPSS software (SPSS Inc., Chicago, IL, USA).

4.3.2 *In Vitro* Suppression of Phosphorylated ERK (pERK) in MCF-7 Cells

The effect on phosphorylated extracellular signal-regulated kinase (pERK) levels in MCF-7 cells was evaluated using a human phospho-ERK1/2 sandwich ELISA kit (Sunlong Biotech Co., Ltd., China) according to the manufacturer's instructions. MCF-7 cells were seeded in 24-well plates at 1×10^5 cells/well and allowed to adhere for 24 h. Cells were then treated with selected active compounds at their respective IC₅₀ concentrations and incubated for an additional 24 h.

Following treatment, culture media were collected, and pERK levels in the supernatants were quantified using the ELISA protocol. Optical density (OD) was measured at 450 nm using a microplate reader. The OD values correlate directly with the concentration of pERK protein in the samples.

4.4 *In-Silico* Investigations

4.4.1 Molecular Docking

Molecular docking studies were performed using PyRx version 8, which integrates AutoDock Vina.⁴¹ The crystal structure of extracellular signal-regulated kinase (ERK) (PDB ID: 5KE0) was obtained from the RCSB Protein Data Bank (<https://www.rcsb.org/>, accessed 28 April 2025).⁴² Prior to docking, the protein structure was prepared by removing water molecules and co-crystallized ligands. The receptor was formatted in PDB using VEGA ZZ, then converted to PDBQT *via* AutoDock Tools.

The reference ligand, 1-[3-(2-methylpyridin-4-yl)-1*H*-pyrazolo[4,3-*c*]pyridin-6-yl]-3-(phenylmethyl)urea (**6S9**), was retrieved from PubChem in SDF format. Test compounds were built using ChemDraw Ultra 10.0, saved as SDF files, and energy-minimized with the MMFF94 force field. Ligands were then converted to PDBQT format using OpenBabel in PyRx.

Docking was conducted by defining a grid box centered at *x* = 47.47, *y* = 12.64, *z* = 8.79 with dimensions 14.90 \times 21.50 \times 15.77 Å, accurately covering the ERK active site. Validation of the docking protocol was confirmed by re-docking the native ligand (**6S9**), yielding an RMSD of 0.0 Å, ensuring methodological accuracy.

Each compound was docked to generate eight poses scored by binding affinity. The most favorable pose with optimal interactions was selected for further analysis. Visualization and interpretation of interactions were performed using BIOVIA

Discovery Studio Visualizer, enabling detailed examination of binding conformations and molecular contacts within the active pocket.

4.4.2 Drug-Likeliness and ADMET Prediction

Drug-likeness and pharmacokinetic properties of top-performing compounds (**3a**, **3b**, and **3d**) were evaluated using SwissADME (<http://www.swissadme.ch/index.php>) and pkCSM (<http://biosig.unimelb.edu.au/pkcsml/>) web platforms.^{43,44} Key physicochemical descriptors—including molecular weight, partition coefficient (LogP), hydrogen bond donors (HBD), hydrogen bond acceptors (HBA), rotatable bonds (nRB), molar refractivity (MR), and topological polar surface area (TPSA)—were assessed following Lipinski's Rule of Five and Veber's guidelines.^{32,22}

These parameters provide comprehensive insights into each compound's oral bioavailability, permeability, and overall drug-like potential. ADMET predictions encompass absorption, distribution, metabolism, excretion, and toxicity profiles, offering preliminary evaluation of pharmacological safety and viability.

References

- Kumar D., Sharma P., Singh H., Nepali K., Gupta G. K., Jain S. K., Ntie-Kang F. (2017) The value of pyrans as anticancer scaffolds in medicinal chemistry. *RSC Advances*, 7, 36977–36999. <https://doi.org/10.1039/C7RA05441F>.
- Kumar A., Jaitak V. (2019) Natural products as multidrug resistance modulators in cancer. *Eur. J. Med. Chem.*, 176, 268–291. <https://doi.org/10.1016/j.ejmech.2019.05.027>.
- Ferlay J., Colombet M., Soerjomataram I., Parkin D. M., Piñeros M., Znaor A., Bray F. (2021) Cancer statistics for the year 2020: An overview. *Int. J. Cancer.*, 149, 778–789. <https://doi.org/10.1002/ijc.33588>.
- Sung H., Ferlay J., Siegel R. L., Laversanne M., Soerjomataram I., Jemal A., Bray F. (2021) Global cancer statistics 2020: GLOBOCAN estimates of incidence and mortality worldwide for 36 cancers in 185 countries. *CA Cancer J. Clin.*, 71, 209–249. <https://doi.org/10.3322/caac.21660>.
- Liu B., Zhou H., Tan L., Siu K. T. H., Guan X.-Y. (2024) Exploring treatment options in cancer: Tumor treatment strategies. *Signal Transduct. Target Ther.*, 9, 175. <https://doi.org/10.1038/s41392-024-01856-7>.
- Punekar S. R., Velcheti V., Neel B. G., Wong K.-K. (2022) The current state of the art and future trends in RAS-targeted cancer therapies. *Nat. Rev. Clin. Oncol.*, 19, 637–655. <https://doi.org/10.1038/s41571-022-00671-9>.
- Boshta N. M., Temirak A., El-Shahid Z. A., Shafiq Z., Soliman A. A. F. (2024) Design, synthesis, molecular docking and biological evaluation of 1,3,5-trisubstituted-1H-pyrazole derivatives as anticancer agents with cell cycle arrest, ERK and RIPK3-kinase activities. *Bioorg. Chem.*, 143, 107058. <https://doi.org/10.1016/j.bioorg.2023.107058>
- Vališ K., Novák, P. (2020) Targeting ERK–Hippo interplay in cancer therapy. *Int. J. Mol. Sci.*, 21, 3236. <https://doi.org/10.3390/ijms21093236>.
- Zhong L., Li Y., Xiong L., Wang W., Wu M., Yuan T., Yang W., Tian C., Miao Z., Wang T., Yang S. (2021) Small molecules in targeted cancer therapy: Advances, challenges, and future perspectives. *Signal Transduct. Target Ther.*, 6, 201. <https://doi.org/10.1038/s41392-021-00572-w>.
- Sebaiy M. M., El-Adl S. M., Nafea A., Mattar A. A., Abdul-Malik M. A., Abdel-Raheem S. A., Elbaramawi S. S. (2024) Review: Instrumental Analytical techniques for Evaluating some Anti-infective Drugs in Pharmaceutical Products and Biological Fluids. *Curr. Chem. Lett.*, 13(3), 491–502.
- Abdel-Megid M., Salem M. E., El-boghdady A. H., El-Rashedy A. A., Abdel-Aal M. T., Nassrallah A., Aboelnaga A., Abouelenein M. G. (2025) Novel Pyrano [2, 3-c] pyrazole Derivatives: Synthesis, Spectroscopic Characterization, and *In Silico* Evaluation of Interactions with VEGFR-1 and Aromatase. *J. Mol. Struct.*, 143107. <https://doi.org/10.1016/j.molstruc.2025.143107>
- Philoppes J. N., Abdelgawad M. A., Abourehab M. A. S., Sebak M., Darwish M. A., Lamie P. F. (2023) Novel N-methylsulfonyl-indole derivatives: Biological activity and COX-2/5-LOX inhibitory effect with improved gastro protective profile and reduced cardiovascular risks. *J. Enzyme Inhib. Med. Chem.*, 38, 246–266. <https://doi.org/10.1080/14756366.2022.2145283>.
- Salerno S., Barresi E., Baglini E., Poggetti V., Da Settimo F., Taliani S. (2023) Target-based anticancer indole derivatives for the development of anti-glioblastoma agents. *Molecules*, 28, 2587. <https://doi.org/10.3390/molecules28062587>.
- Luo M.-L., Huang W., Zhu H.-P., Peng C., Zhao Q., Han B. (2022) Advances in indole-containing alkaloids as potential anticancer agents by regulating autophagy. *Biomed. Pharmacother.*, 149, 112827. <https://doi.org/10.1016/j.biopha.2022.112827>.
- Jia Z., Zhang Z., Tian Q., Wu H., Xie Y., Li A., Zhang H., Yang Z., Zhang X. (2021) Integration of transcriptomics and metabolomics reveals anlotinib-induced cytotoxicity in colon cancer cells. *Gene.*, 786, 145625. <https://doi.org/10.1016/j.gene.2021.145625>.
- Lu J., Zhong H., Chu T., Zhang X., Li R., Sun J., Zhong R., Yang Y., Alam M. S., Lou Y., Xu J., Zhang Y., Wu J., Li X., Zhao X., Li K., Lu L., Han B. (2019) Role of anlotinib-induced CCL2 decrease in anti-angiogenesis and

- response prediction for nonsmall cell lung cancer therapy. *Eur. Respir. J.*, 53, 1801562. <https://doi.org/10.1183/13993003.01562-2018>.
- 17 Oxnard G. R., Hu Y., Mileham K. F., Husain H., Costa D. B., Tracy P., Feeney N., Sholl L. M., Dahlberg S. E., Redig A. J., Kwiatkowski D. J., Rabin M. S., Paweletz C. P., Thress K. S., Jänne P. A. (2018) Assessment of resistance mechanisms and clinical implications in patients with EGFR T790M-positive lung cancer and acquired resistance to osimertinib. *JAMA Oncol.*, 4, 1527. <https://doi.org/10.1001/jamaoncol.2018.2969>.
- 18 Camidge D. R., Dziadziuszko R., Peters S., Mok T., Noe J., Nowicka M., Gadgeel S. M., Cheema P., Pavlakis N., de Marinis F., Cho B. C., Zhang L., Moro-Sibilot D., Liu T., Bordogna W., Balas B., Müller B., Shaw A. T. (2019) Updated efficacy and safety data and impact of the EML4-ALK fusion variant on the efficacy of alectinib in untreated ALK-positive advanced non-small cell lung cancer in the global phase III ALEX study. *J. Thorac. Oncol.*, 14, 1233–1243. <https://doi.org/10.1016/j.jtho.2019.03.007>.
- 19 Gupta O., Pradhan T., Chawla G. (2023) An updated review on diverse range of biological activities of 1,2,4-triazole derivatives: Insight into structure–activity relationship. *J. Mol. Struct.*, 1274, 134487. <https://doi.org/10.1016/j.molstruc.2022.134487>.
- 20 Czyski A., Resztak M., Świdorski P., Brylak J., Główna F. K. (2021) The overview on the pharmacokinetic and pharmacodynamic interactions of triazoles. *Pharmaceutics*, 13, 1961. <https://doi.org/10.3390/pharmaceutics13111961>.
- 21 Aitouna A. O., Syed A., Alfagham A. T., Mazoir N., de Julián-Ortiz J. V., Elgorban A. M., El Idrissi M., Wong S. L., Zeroual, A. (2024) Investigating the chemical reactivity and molecular docking of 2-diazo-3, 3, 3-trifluoro-1-nitropropane with phenyl methacrylate using computational methods. *Chem. Heterocycl. Compd.*, 60 (11), 592–599. <https://doi.org/10.1007/s10593-025-03382-y>
- 22 Klenina O. V., Chaban T. I., Chaban I. H., Lelyukh M. I. (2025) Recent advances in the synthesis of thiazolo [4, 5-*b*] pyridines. Part 3. Focus on biological activity (microreview). *Chem. Heterocycl. Compd.*, 61 (1/2) 1-4. <https://doi.org/10.1007/s10593-025-03398-4>
- 23 Ameer S., Barhoumi A., Abdallaoui H. E. A. E., Syed A., Belghiti M. E., Elgorban A. M., Wong S. L., Wang S., El Idrissi M., Zeroual A., Mazoir, N. (2024) Molecular docking, exploring diverse selectivities and mechanistic insights in the cycloaddition reaction between 3-benzoylpyrrolo-[1, 2-*a*] quinoxaline-1, 2, 4 (5H)-triones and butyl vinyl ether. *Chem. Heterocycl. Compd.*, 60 (11), 584–591. <https://doi.org/10.1007/s10593-025-03381-z>
- 24 Yele V., Pindiprolu S. K. S. S., Sana S., Ramamurthy D. S. V. N. M., Madasi J. R. K., Vadlamani, S. (2021) Synthesis and preclinical evaluation of indole triazole conjugates as microtubule targeting agents that are effective against MCF-7 breast cancer cell lines. *Anticancer Agents Med. Chem.*, 21, 1047–1055. <https://doi.org/10.2174/1871520620666200925102940>.
- 25 Zahoor A. F., Saeed S., Rasul A., Noreen R., Irfan A., Ahmad S., Faisal S., Al-Hussain S. A., Saeed M. A., Muhammed M. T., Muhammad Z. A., Zaki M. E. A. (2023) Synthesis, cytotoxic, and computational screening of some novel indole–1,2,4-triazole-based *S*-alkylated *N*-aryl acetamides. *Biomedicines*, 11, 3078. <https://doi.org/10.3390/biomedicines11113078>.
- 26 Abouelenein M. G., El-Rashedy A. A., Awad H. M., El Farargy A. F., Nassar I. F., Nassrallah, A. (2023) Synthesis, molecular modeling insights, and anticancer assessment of novel polyfunctionalized pyridine congeners. *Bioorg. Chem.*, 141, 106910. <https://doi.org/10.1016/j.bioorg.2023.106910>.
- 27 Abouelenein M. G., Mohamed M. B. I., Elsenety M. M., El-Rashedy A. A., Ghalib S. H., Mohamed F. A. E., El-Ebiary N. M. A., Ageeli A. A. (2024) Facile and novel synthetic approach, molecular docking, molecular dynamics, and drug-likeness evaluation of 9-substituted acridine derivatives as dual anticancer and antimicrobial agents. *Chem. Biodivers.*, 21. <https://doi.org/10.1002/cbdv.202301986>.
- 28 Abo-Salem H. M., Gibriel A. A., El Awady M. E., Mandour A. H. (2020) Synthesis, molecular docking and biological evaluation of novel flavone derivatives as potential anticancer agents targeting Akt. *Med. Chem. (Los Angeles)*, 17, 158–170. <https://doi.org/10.2174/1573406416666200306115035>.
- 29 Fawzy N. M., Ahmed K. M., Abo-Salem H. M., Aly M. S. (2022) Novel furochromone derivatives of potential anticancer activity targeting EGFR tyrosine kinase: Synthesis and molecular docking study. *Russ. J. Bioorg. Chem.*, 48, 749–767. <https://doi.org/10.1134/S1068162022040082>.
- 30 Abo-Salem H. M., El Souda S. S. M., Shafey H. I., Zoheir K. M. A., Ahmed K. M., Mahmoud Kh., Mahrous K. F., Fawzy N. M. (2024) Synthesis, bioactivity assessment, molecular docking and ADMET studies of new chromone congeners exhibiting potent anticancer activity. *Sci. Rep.*, 14, 9636. <https://doi.org/10.1038/s41598-024-59606-2>.
- 31 Abdelmegeed H., Abo-Salem H. M., Zayed E. M., El-Sawy E. R. (2024) Anti colorectal cancer activity and in silico studies of novel pyridine nortopsentin analog as cyclin dependent kinase 6 inhibitor. *Sci. Rep.*, 14, 26327. <https://doi.org/10.1038/s41598-024-75411-3>.
- 32 Lipinski C. A. (2004) Lead- and drug-like compounds: the rule-of-five revolution. *Drug Discov. Today Technol.*, 1, 337–341. <https://doi.org/10.1016/j.ddtec.2004.11.007>.
- 33 Veber D. F., Johnson S. R., Cheng H.-Y., Smith B. R., Ward K. W., Kopple K. D. (2002) Molecular properties that influence the oral bioavailability of drug candidates. *J. Med. Chem.*, 45, 2615–2623. <https://doi.org/10.1021/jm020017n>.
- 34 Al-blewi F. F., Almeahmadi M. A., Aouad M. R., Bardaweel S. K., Sahu P. K., Messali M., Rezki N., El Ashry E. S. H. (2018) Design, synthesis, ADME prediction and pharmacological evaluation of novel benzimidazole-1,2,3-

- triazole-sulfonamide hybrids as antimicrobial and antiproliferative agents. *Chem. Cent. J.*, 12, 110. <https://doi.org/10.1186/s13065-018-0479-1>.
- 35 Flores-Holguín N., Frau J., Glossman-Mitnik D. (2021) In silico pharmacokinetics, ADMET study and conceptual DFT analysis of two plant cyclopeptides isolated from Rosaceae as a computational peptidology approach. *Front. Chem.*, 9. <https://doi.org/10.3389/fchem.2021.708364>.
- 36 Pires D.E.V., Blundell T.L., Ascher D.B. (2015) pkCSM: Predicting small-molecule pharmacokinetic and toxicity properties using graph-based signatures. *J. Med. Chem.*, 58, 4066–4072. <https://doi.org/10.1021/acs.jmedchem.5b00104>.
- 37 Seville L., Gavara L., Bebrone C., De Luca F., Nauton L., Achard M., Mercuri P., Tanfoni S., Borgianni L., Guyon C., Lonjon P., Turan-Zitouni G., Dzieciolowski J., Becker K., Bénard L., Condon C., Maillard L., Martinez J., Frère J., Dideberg O., Galleni M., Docquier J., Hernandez J. (2017) 1,2,4-Triazole-3-thione compounds as inhibitors of dizinc metallo- β -lactamases. *Chem. Med. Chem.*, 12, 972–985. <https://doi.org/10.1002/cmdc.201700186>.
- 38 Souza H., de Sousa R., Lira B., Vilela R., Borges N., de Siqueira Junior J., Lima E., Jardim J., da Silva G., Barbosa Filho J., de Athayde Filho P. (2018) Synthesis, in silico study and antimicrobial evaluation of new selenoglycolicamides. *J. Braz. Chem. Soc.* <https://doi.org/10.21577/0103-5053.20180148>
- 39 Liu K., Zhu C., Liang Y., Min D., Jin Z., Sun X. (2025) Discovery of a novel 1,4-benzodiazepine derivative as a highly selective ANXA3 degrader for the treatment of triple-negative breast cancer. *J. Med. Chem.*, 68, 5358–5381. <https://doi.org/10.1021/acs.jmedchem.4c02403>.
- 40 Li Q., Lou Z., Wang C., Li Y. (2025) In vitro anticancer effects in hepatocellular carcinoma (HCC) and protein interaction study of xanthoangelol. *Int. J. Biol. Macromol.*, 302, 138530. <https://doi.org/10.1016/j.ijbiomac.2024.138530>
- 41 Trott O., Olson A. J. (2010) AutoDock Vina: Improving the speed and accuracy of docking with a new scoring function, efficient optimization, and multithreading. *J. Comput. Chem.*, 31 (2), 455–461. <https://doi.org/10.1002/jcc.21334>
- 42 Lim J., Kelley E. H., Methot J. L., Zhou H., Petrocchi A., Chen H., Hill S. E., Hinton M. C., Hruza A., Jung J. O., Maclean J. K. F., Mansueto M., Naumov G. N., Philippar U., Raut S., Spacciapoli P., Sun D., Siliphaivanh P. (2016) Discovery of 1-(1H-pyrazolo[4,3-c]pyridin-6-yl)urea inhibitors of extracellular signal-regulated kinase (ERK) for the treatment of cancers. *J. Med. Chem.*, 59 (14), 6501–6511. <https://doi.org/10.1021/acs.jmedchem.6b00708>.
- 43 Daina A., Michielin O., Zoete V. (2017) SwissADME: A free web tool to evaluate pharmacokinetics, drug-likeness and medicinal chemistry friendliness of small molecules. *Sci. Rep.*, 7, 42717. <https://doi.org/10.1038/srep42717>
- 44 Pires D. E. V., Blundell T. L., Ascher D. B. (2015) pkCSM: Predicting small-molecule pharmacokinetic and toxicity properties using graph-based signatures. *J. Med. Chem.*, 58 (9), 4066–4072. <https://doi.org/10.1021/acs.jmedchem.5b00104>.



© 2025 by the authors; licensee Growing Science, Canada. This is an open access article distributed under the terms and conditions of the Creative Commons Attribution (CC-BY) license (<http://creativecommons.org/licenses/by/4.0/>).